

## Article

# Investigation on the Influences of Hygrothermal Aging on the Indentation Size Effects and Micro-Indentation Measurements of PMMA. Part I: Experimental Results

Hui Lin <sup>1,2,\*</sup>, Lin Lv <sup>1</sup> and Tao Jin <sup>3,4</sup>

<sup>1</sup> College of automobile, Hangzhou Vocational & Technical College, Hangzhou 310018, China; lvlin@hzvtc.edu.cn

<sup>2</sup> Key Laboratory of E&M, Ministry of Education & Zhejiang Province, Zhejiang University of Technology, Hangzhou 310014, China

<sup>3</sup> Institute of Applied Mechanics, Taiyuan University of Technology, Taiyuan 030024, China; jintao@tyut.edu.cn

<sup>4</sup> State Key Laboratory for Strength and Vibration of Mechanical Structures, Xi'an Jiaotong University, Xi'an 710049, China

\* Correspondence: linhui@hzvtc.edu.cn

Received: 15 July 2020; Accepted: 4 August 2020; Published: 7 August 2020



**Abstract:** The polymethyl methacrylate (PMMA) subjected to hygrothermal aging was applied to nanoindentation tests under different indentation strain rates. The influences of hygrothermal aging on the indentation behaviors of PMMA are discussed. Results show that the indentation elastic modulus and hardness decrease with increasing aging time. Furthermore, the indentation size effects (ISE) can be observed in aged PMMA specimens as they are sensitive to aging time as well as to the indentation strain rate. The quantitative analysis of ISE is proposed on the basis of shear transformation-mediated plasticity and was presented in our companion paper.

**Keywords:** pressure-sensitive polymer; indentation size effects; strength differential (SD) effects; shear transformation-mediated plasticity; hygrothermal aging

## 1. Introduction

Polymethyl methacrylate (PMMA) is extensively applied in different industrial areas, such as aircraft, automotive industries, and biomedical materials, for its excellent properties [1–6]. For these widely used materials, mechanical strength is the first and foremost characteristic to ensure safety [7–12]. Therefore, many studies focused on the common mechanical properties, i.e., compression [2,13], tension [14], and shear [2], of PMMA. Besides, some studies raise concerns on the mechanical responses of PMMA under complex stress states, such as combined loading conditions [13–16]. The mechanical behaviors of PMMA under combined stress states always differ to that under uniaxial loading because of the introduction of additional shear stress. The yielding and failure of PMMA are sensitive to shear stress, i.e., the introduced shear stress decreases its normal stress strength. Many studies focus on the instrumented indentation behaviors of PMMA due to its increasing applications in microelectromechanical systems, i.e., the improved capabilities of recent instruments. Thus, tests should be performed on a small volume of materials [17,18]. However, the phenomenon in which the mechanical properties of materials with a small volume are always enhanced compared with those with large volume is called the indentation size effects (ISE). The indentation hardness of tested materials, caused by the strain gradients, usually depends on the indentation depth and increases with decreasing depth [19–21]. For metallic materials, ISE can be characterized by the statistically stored

dislocations and the geometrically necessary dislocations, which grow with the plastic strain, and are produced by the heterogeneous plastic flow attributable to the gradients of plastic strain [22–24]. These concepts are widely accepted to describe the ISE in crystalline materials. However, the PMMA as glass polymer (GPs) is a typical amorphous material that has a significantly different deformation mechanism compared with other crystalline materials. Therefore, the dislocation-mediated plasticity may not be suitable for describing the ISE in GPs. By contrast, the cooperative-localized rearrangement of atomic or molecular clusters in small distinct regions, defined as shear transformation-mediated plasticity, is a widely accepted mechanism for plastic deformation in GPs [1]. As displayed by Voyiadjis et al. [17,23,25], shear transformation-mediated plasticity has been successfully applied in the modeling of ISE in PMMA and PC (College of automobile).

The mechanical behaviors of such materials are always sensitive to the loading conditions, such as strain rate, temperature, light, and humidity [5,26–29]. The yield strength always increases with the strain rate, and the opposite is true for temperature [30]. This finding means that the correlation between the mechanical behaviors of material with environmental conditions is an important issue. This is because the mechanical behavior of PMMA is sensitive to heat. Moreover, the heat can aggravate the molecular motion of PMMA, resulting in more moisture intruding into the free volume of glassy state PMMA through the surface micro-voids. Then, the intruded water molecules will be combined with the hydrophilic groups, such as methyl groups in PMMA through hydrogen bonds. Therefore, the mechanical properties of PMMA under the condition of hygrothermal aging are quite different from that without hygrothermal treatment. Furthermore, the evolution of the mechanical behaviors of materials during aging is also an important parameter to judge or evaluate the useful life of materials in practical applications. However, as mentioned above, ISE, which cannot be avoided in materials during indentation test, has been clarified in normal test conditions for PMMA.

This paper aimed to study the indentation behavior of aged PMMA. Then, the sensitivity of mechanical behaviors to hygrothermal aging, such as ISE, elastic modulus, and hardness can be analyzed. The preparation of samples and nanoindentation tests are presented in Section 2. The indentation results are shown in Section 3. The ISE modeling of aged PMMA is analyzed in Section 4. Finally, the conclusions are given in Section 5. This paper focuses on the experimental results of aged PMMA under indentation with different strain rates, and the related theoretical analysis and modeling are displayed in our companion paper.

## 2. Experimental

### 2.1. Materials

Commercial grade materials were purchased from Degussa AG Plexiglas® PMMA. PMMA was prepared through a traditional cell cast method. Thus, no molecular chain orientation existed in the as-cast sheet, and the PMMA can be regarded as isotropic material.

The cube specimens with a size of 20 mm × 20 mm × 5 mm were used in the nanoindentation tests. The laser cutting method was used to prepare the specimens from the semifinished product of bulk PMMA. A chamber with constant temperature and humidity (SDH-401, Hengda, Chongqing, China) was applied to the damp heat test. Then, the effects of hygrothermal aging on the mechanical behaviors of PMMA can be investigated. In accordance with the GB/T 10586-2006, the PMMA specimens were subjected to 85 °C and 85% relative humidity with different aging times (0, 240, 312, 600, and 720 h).

### 2.2. Indentation Tests

A nanoindenter test system (G200, Agilent Technologies, CA, USA) with triangular pyramid Berkovich diamond indenter was used to characterize the mechanical behaviors of PMMA specimens. The continuous hardness and elastic modulus with indentation depth can be obtained through the continuous stiffness measurement (CSM) technique, and the indentation tests were carried out at different loading rates ( $\dot{P}$ ; i.e., 0.05, 0.1, and 0.2 s<sup>−1</sup>). The detailed technical parameters can be found

in our previous paper [1]. The principle of the CSM technique of nanoindentation has been widely reported in various studies [1,31,32] and will not be repeated in this paper. Furthermore, each test was performed at room temperature (25 °C) and repeated 3–4 times on the different locations of same specimen surface to exclude contingency factors. Figure 1 shows the three results of force-depth curves of aged (720 h) PMMA specimens under indentation with the highest  $\dot{P}/P$  ( $0.2 \text{ s}^{-1}$ ). Three different tests obtained almost the same results. Therefore, the indentation tests in this paper were reliable, and the contingency factors can be neglected. Based on the constant indentation force-depth curve at different locations of the tested PMMA samples, the PMMA specimens with aging treatment were considered to be homogeneous.

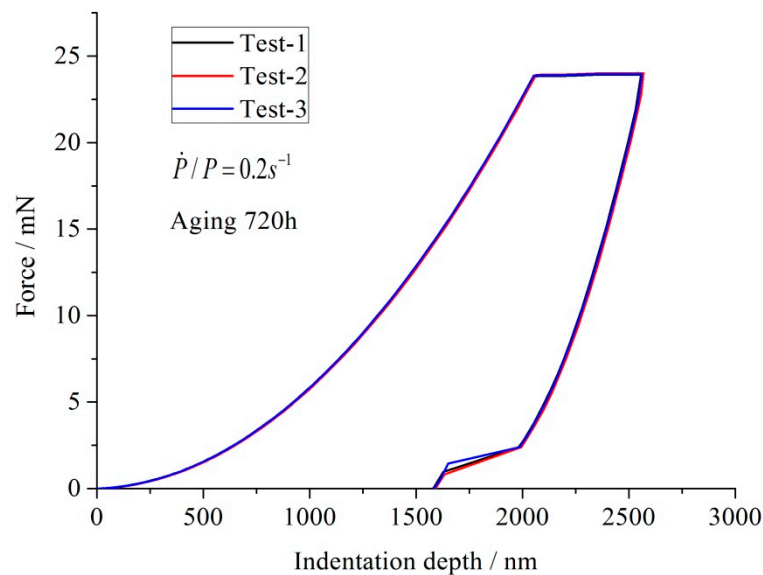


**Figure 1.** Repeated nanoindentation tests of the aged polymethyl methacrylate (PMMA) specimens.

Figure 1 shows the typical indentation force-depth curve which includes the loading, holding, and unloading stages. The maximum indentation depth was set as 2000 nm. The force nonlinearly increased with the increasing depth until it reached 2000 nm, indicating the end of the loading stage. The holding stage indicated that the force remained at the corresponding peak load for 100 s to release creep deformation. During the unloading stage, the load was unloaded to  $0.1P_{\max}$  for thermal drift correction and then dropped to 0, indicating the end of the indentation test.

### 3. Results

#### 3.1. Load History During Loading Stage

The  $\dot{P}/P = a$  is a constant during the indentation process when CSM is used. For the constant  $a$ , the loading function set in the indentation system is [33]:

$$P = Ae^{at} \quad (1)$$

where  $P$ ,  $A$ , and  $t$  are the force, constant, and time, respectively.  $P$  and  $t$  can be recorded using the indentation system during the indentation process (Figure 2). The time to reach a certain force is shortened with increasing  $\dot{P}/P$ . A high force is needed for a large  $a$  when the same indentation depth is reached. Since the loading stage with a large  $a$  does not have enough time to release the viscous deformation, the molecular chain segments under the indenter deform under the external force. The force history under different loading conditions can be fitted based on the above equation, and the parameter  $A$  is listed in Table 1. The value of  $a$  decreases with increasing  $\dot{P}/P$ . Furthermore, the value

of a varies with aging time, which indicates that the mechanical properties of PMMA can be affected by aging. Therefore, the influence of hygrothermal aging on mechanical behaviors should be analyzed.

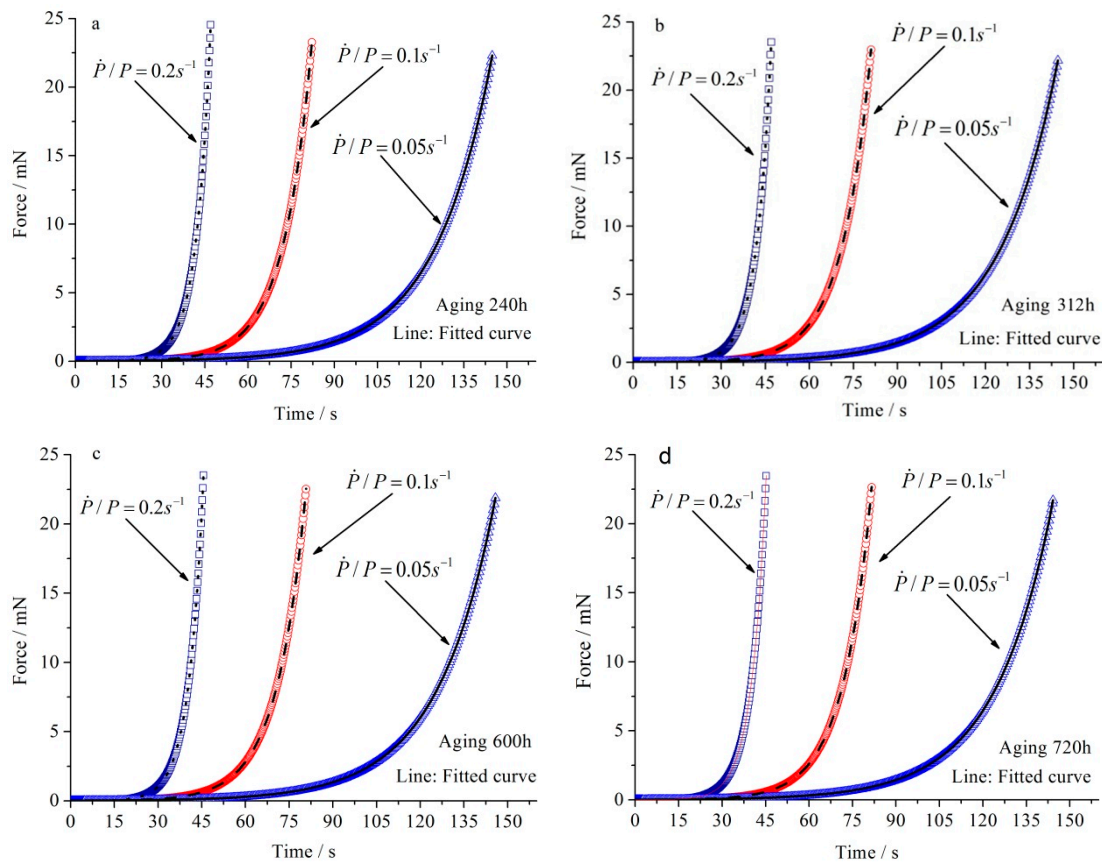


**Figure 2.** Force-time curves at the loading stage of the aged PMMA specimens under nanoindentation at aging times of 240 (a), 312 (b), 600 (c), and 720 (d) h.

**Table 1.** Fitted parameter A of the aged PMMA under different loading rates.

$\dot{P}/P$ (s <sup>-1</sup> )	Aging Time (h)			
	240	312	600	720
0.05	0.016	0.016	0.015	0.016
0.1	0.00627	0.00698	0.00698	0.00648
0.2	0.00204	0.00195	0.00258	0.00279

### 3.2. Indentation Strain Rate ( $\dot{\epsilon}_i$ )

The ISE under different conditions must be clarified before the effects of strain rate and aging time on the indentation mechanical properties of PMMA are analyzed, and the characteristic depth marked as  $d_{sp}$  is defined as the critical depth that the mechanical properties of PMMA no longer depend on the depth. Moreover, it can be used to represent the mechanical properties of the bulk material. Moreover, no explicit evidence shows that aging has no effect the PMMA ISE. This finding also indicates that the statement  $d_{sp} = 1000$  nm in our previous paper [1] cannot be used directly in this paper. Therefore, the effects of hygrothermal aging on the ISE of PMMA must be understood. Based on the investigation of the ISE of unaged PMMA in our previous paper [1], shear transformation-mediated plasticity is utilized to explain the plastic deformation of amorphous materials [34]. Additionally, the Arrhenius equation [35,36] is applied to correlate the indentation

effective shear strain rate ( $\dot{\gamma}$ ), shear yield stress ( $\tau_s$ ), activation energy ( $\Delta F_0$ ), shear strain of Shear transformation zone (STZ) ( $\gamma^T = 0.04$ ), and activation volume ( $\Omega$ ):

$$\dot{\gamma} = \varnothing_{ss} \gamma^T v_G \exp\left(-\frac{\Delta F_0}{k_B T}\right) \sinh\left(\frac{\gamma^T \Omega \tau_s}{2k_B T}\right) \quad (2)$$

where  $k_B$ ,  $T$ , and  $\varnothing_{ss}$  are the Boltzmann constant, absolute temperature, and a constant set to 0.5 for plastic state, respectively.  $v_G = 10^{10} \text{ s}^{-1}$  is the attempt frequency. The shear transformation-mediated plasticity is introduced in detail in many existing articles [1,17,25]. Thus, reintroduction is not needed. The  $\dot{\gamma}$  in the Arrhenius equation is the shear strain rate, rather than  $\dot{P}/P$  or  $\dot{\epsilon}_i = \frac{dh}{hdt}$ .  $\dot{\epsilon}_i$  can be controlled by setting different  $\dot{P}/P$  values. In the indentation tests, the indentation effective  $\dot{\gamma}$  can be calculated [17,25]:

$$\dot{\gamma} = \sqrt{3} C \dot{\epsilon}_i \quad (3)$$

where  $C$  is 0.09 [37–39]. The  $\dot{\gamma}$  of the aged PMMA can be obtained during indentation (Figure 3) and decreases with increasing indentation depth until a convergence value is reached. In addition, the  $\dot{\gamma}$  values of 0.004, 0.008, and 0.016  $\text{s}^{-1}$  correspond to the  $\dot{P}/P$  values of 0.05, 0.1, and 0.2  $\text{s}^{-1}$ , respectively, which is consistent with the result of the unaged PMMA. Aging time can also be considered to have almost no effect on it by the comparison of indentation results between unaged and aged PMMA because the indentation conditions are the same. For convenience, the effective indentation  $\dot{\gamma}$  is simplified into strain rate (SR) in the following text.

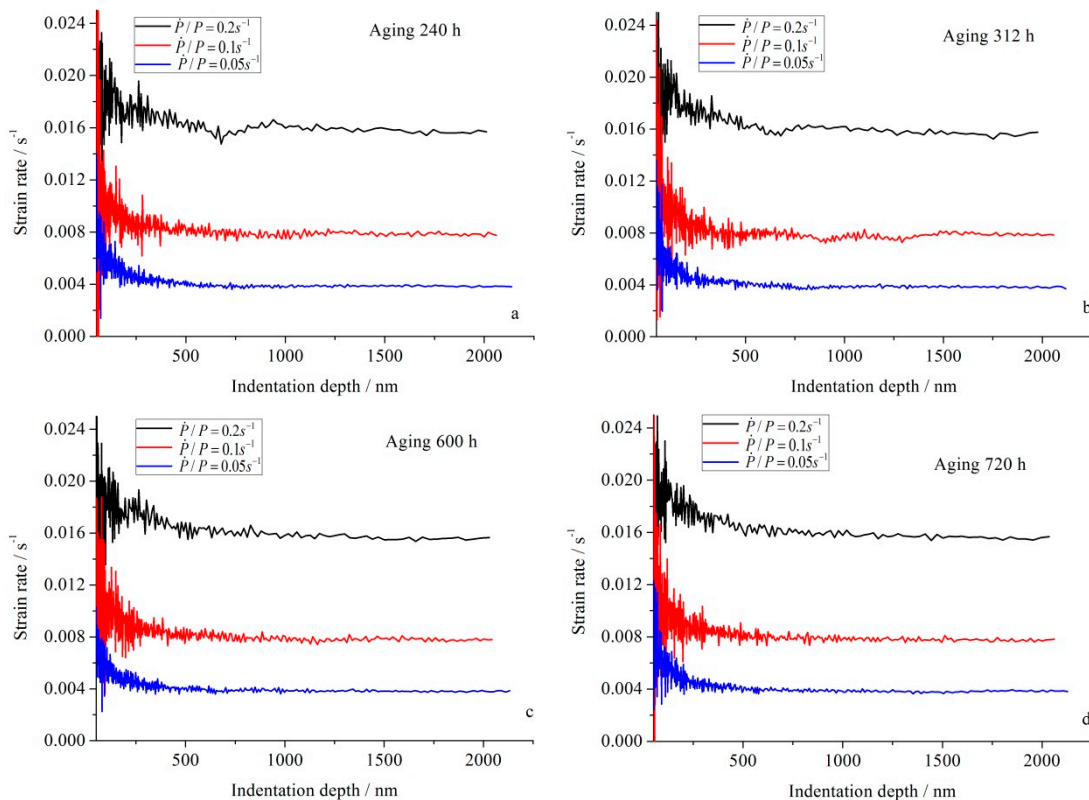


**Figure 3.** Variation in the shear strain rate vs. the depth of the aged PMMA with different aging times: (a) 240 h, (b) 312 h, (c) 600 h and (d) 720 h.

The continuous contact stiffness can be obtained by using CSM (Figure 4). The contact stiffness  $S$  almost increases linearly with the increasing depth  $h$ . Cheng et al. gave the theoretical explanation i.e.,  $S \propto h$  [40] based on the dimension analysis. In addition, the slope of  $S$ – $h$  can be regarded as the



elastic property of the materials to a certain degree. Moreover, the slope was found to be positively correlated with SR, which indicates that the aged PMMA exhibits the strain rate sensitivity like unaged PMMA [31].

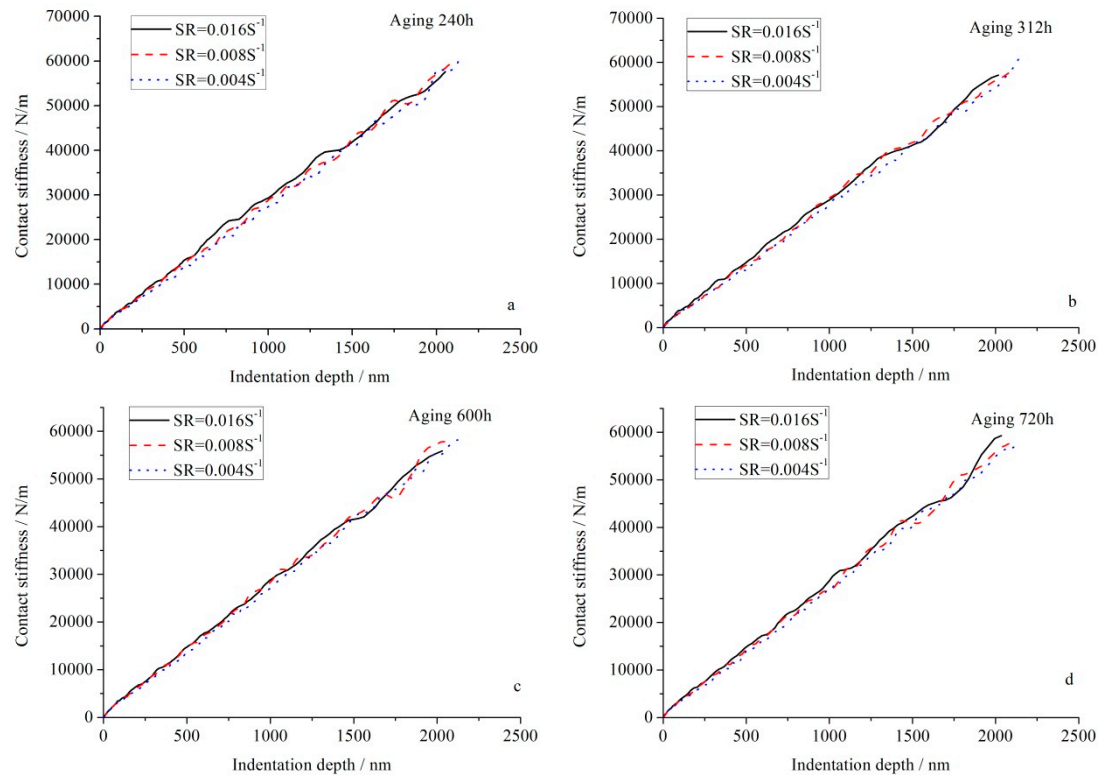
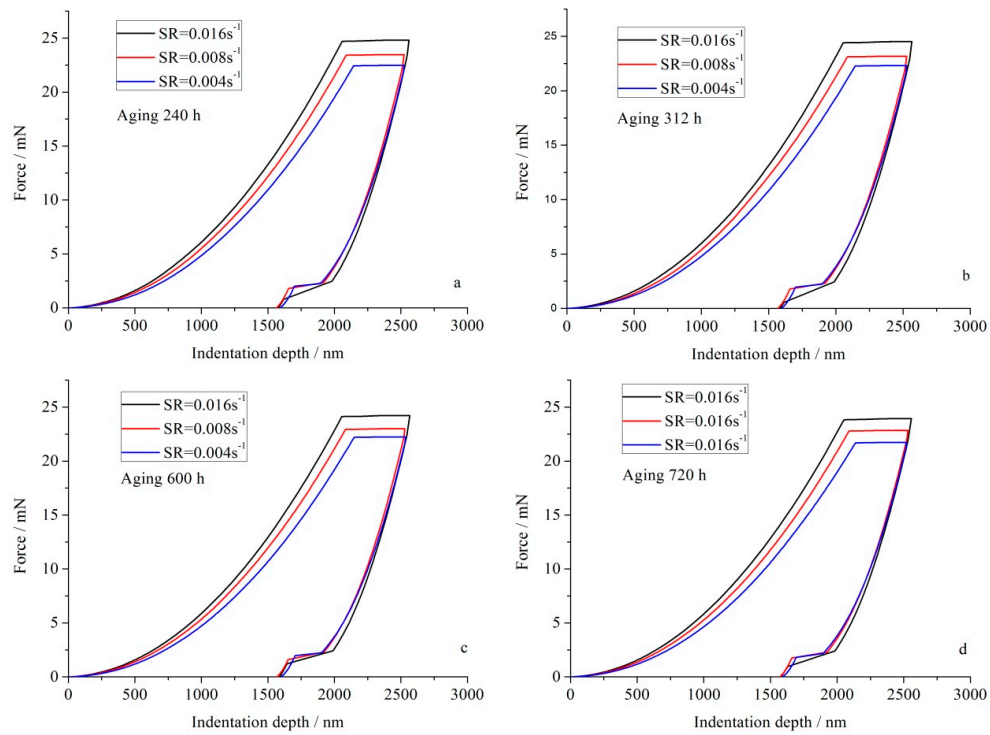


**Figure 4.** Contact stiffness of the PMMA specimens after processing at the different aging times: (a) 240 h, (b) 312 h, (c) 600 h and (d) 720 h.

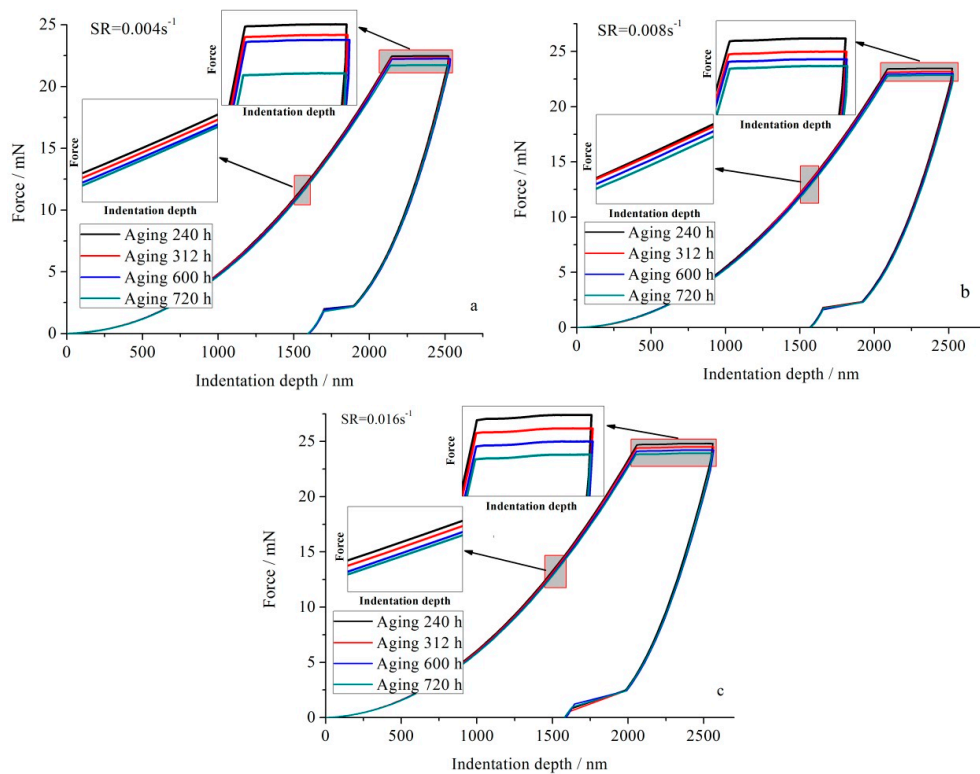
### 3.3. Force-Depth Curve

Figure 5 shows the force-depth curves of the aged PMMA under three different SRs. A higher force is needed for the loading condition with a larger SR at the same indentation displacement during the loading stage, which results from the time-dependent deformation (viscous effect) of the material. The SR in this paper belongs to the quasistatic range, and the load method does not involve any dynamic device. Therefore, the inertial effect or inertial force can be ignored during the analysis process.

Figure 6 displays the effects of aging time on the indentation force-depth curves of PMMA. From the entire force-depth curve, the aging time has no evident effect on the indentation response of PMMA. However, the differences between the indentation responses of PMMA after aging at various aging times become observable, as displayed in the plot of the partial enlargement of the loading and holding stages. Furthermore, the increased speed of indentation force with depth during the loading stage reduces with aging time, which is similar to the SR effects. The force at the maximum indentation depth of 2000 nm also decreases with increasing aging time. The SR effects of PMMA are due to the nature of the material and some physical properties of PMMA have been changed by hygrothermal aging.



**Figure 5.** Force-depth curves of the PMMA specimens under three strain rates after processing at different aging times: (a) 240 h, (b) 312 h, (c) 600 h and (d) 720 h.

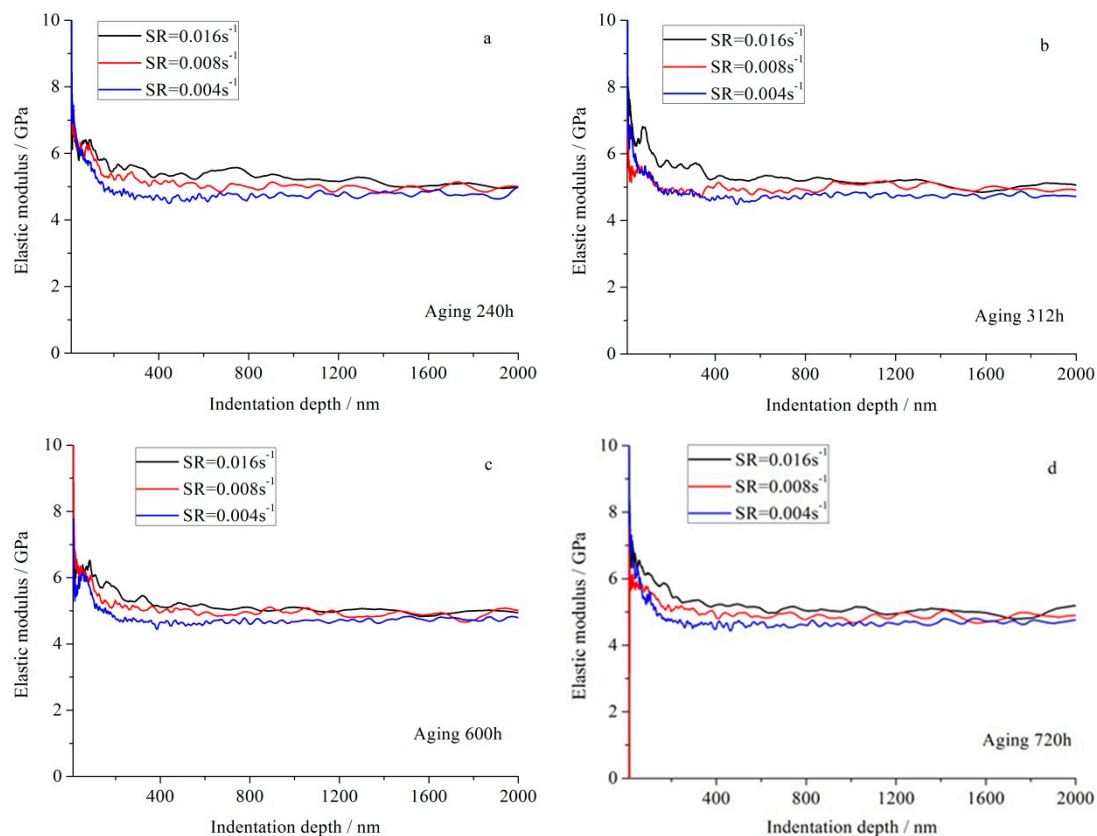


**Figure 6.** Effects of aging time on the indentation force-depth curves of PMMA under different SRs: (a)  $0.004 \text{ s}^{-1}$ , (b)  $0.008 \text{ s}^{-1}$  and (c)  $0.016 \text{ s}^{-1}$ .

### 3.4. Indentation Elastic Modulus and Hardness

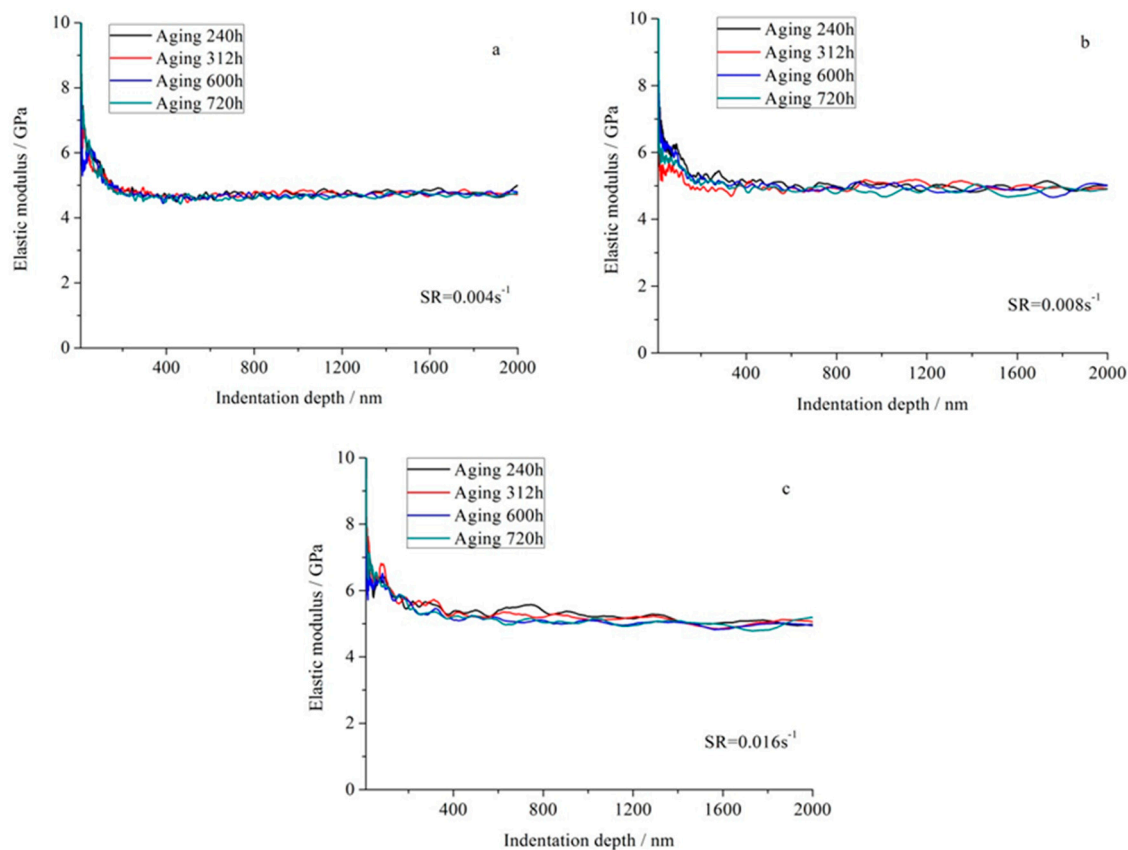
The continuous elastic modulus during the loading stage can be obtained (Figure 7). The elastic modulus of aged PMMA exhibits evident ISE, decreases with depth and then stabilizes. The stable elastic modulus increases with SR, which further illustrates its sensitivity to strain rate. Figure 8 displays the continuous indentation elastic modulus of PMMA after aging at different times. The continuous modulus of different aging times overlap and the effects of aging time cannot be illustrated intuitively in Figure 8. Therefore, the arithmetic mean value of the elastic modulus at a certain depth range is applied to characterize the mechanical behavior of aged PMMA. Thus, the ISE of aged PMMA should be analyzed to find the characteristic depth to determine the depth range, in which the ISE can be neglected.

Figure 9 shows the hardness history during the loading stage of the aged PMMA under three different SRs. The hardness of the aged PMMA exhibits a significant dependence on the indentation depth. In addition, the ISE of hardness is normal, i.e., the hardness increases with decreasing depth. For a same aged specimen, the characteristic depth increases with SR, which is similar to the unaged PMMA and can be observed roughly in Figure 9. Beyond the characteristic depth, the hardness also converges to a stable value. The stable hardness is also proportional to SR, which is similar to the elastic modulus. The above analysis about the ISE of PMMA is qualitative, and the quantitative characteristic depth still cannot be obtained.



**Figure 7.** Continuous elastic modulus of the PMMA specimens under the three strain rates after processing at different aging times: (a) 240 h, (b) 312 h, (c) 600 h and (d) 720 h





**Figure 8.** Effects of aging time on the continuous indentation elastic modulus of PMMA under different SRs: (a)  $0.004 \text{ s}^{-1}$ , (b)  $0.008 \text{ s}^{-1}$  and (c)  $0.016 \text{ s}^{-1}$ .

Figure 10 displays the hardness history of the PMMA after aging at different times. For each SR, the stable hardness decreases with the increasing aging time. This finding means that hygrothermal aging degrades the mechanical behaviors of PMMA specimens. Based on the indentation results, within the time range involved in this paper, prolonged aging time worsens the mechanical properties of the material. A further quantitative relationship between the aging time and mechanical properties of PMMA can be confirmed after determining the  $\Omega_{st}$  and  $\chi$ .  $\Omega_{st}$  is the volume of STz (STz size), and  $\chi$  is the total probability of finding a fertile zone that can undergo discrete shear transformation within the deformation zone. These parameters are applied to analyze the ISE of aged PMMA through shear transformation-mediated plasticity, and the detailed description will be displayed in our companion paper.

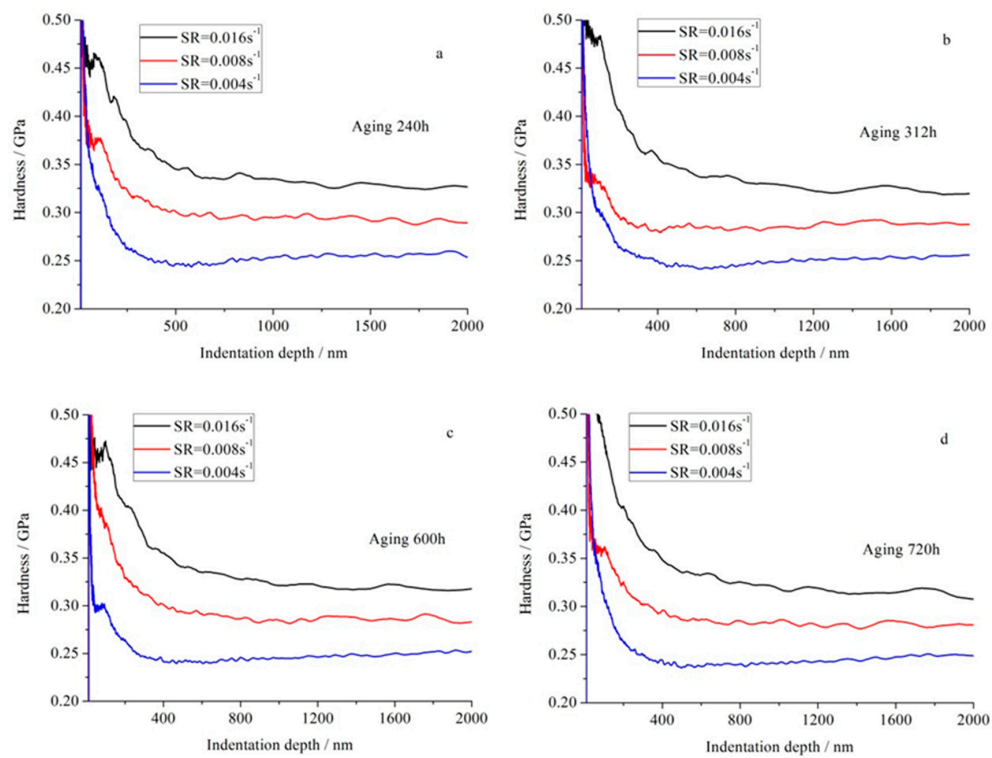


**Figure 9.** Continuous hardness of the PMMA specimens under the three strain rates after processing at different aging times: (a) 240 h, (b) 312 h, (c) 600 h and (d) 720 h.

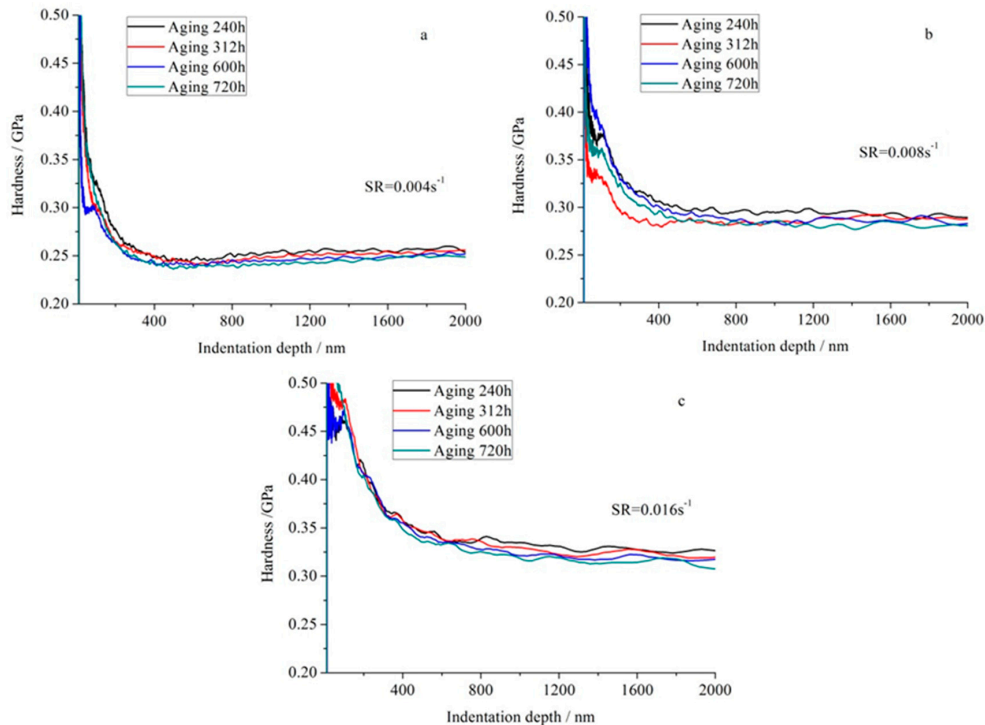


**Figure 10.** Effect of the aging time on the continuous indentation hardness of PMMA under different SRs: (a)  $0.004 \text{ s}^{-1}$ , (b)  $0.008 \text{ s}^{-1}$  and (c)  $0.016 \text{ s}^{-1}$ .

#### 4. Discussions

The nanoindentation results of aged specimens can be obtained directly from the test machine. The average values of the elastic modulus and hardness based on a certain range of indentation depth (preset by tester) can be provided accordingly. The subsequent quantitative analysis of the effects of hygrothermal aging on PMMA indentation mechanical behaviors can be carried out after the reliability of the provided modulus and hardness is confirmed. This is because the existence of the ISE of aged specimens is still uncertain, despite the fact that the ISE of unaged PMMA has been clarified in our previous paper [1]. Based on the above description, the quantitative effects of hygrothermal aging on PMMA indentation's mechanical properties can be only understood if the  $d_{sp}$  can be determined, which marks the minimum depth for which the tested hardness and modulus can be used for representing its bulk properties. Thus, the whole indentation process of aged PMMA should be analyzed, and the depth that indicates the disappearance of ISE should be determined. Similar to our previous paper, shear transformation-mediated plasticity is used to describe the ISE of the aged PMMA in the companion paper and the transformation-mediated plasticity theory is introduced by Voyiadjis in detail [17,23,25].

The total shear stress of the tested area of PMMA under the indenter ( $\tau_{local}$ ) results from the shear stress associated with formation of a single STz ( $\tau_{st}$ ) and the shear stress associated with the plastic deformation of the highly stressed region  $\tau_{local}$ . The weight coefficient ( $\chi$ ) is used to balance the contribution of  $\tau_{local}$  and  $\tau_{st}$  to  $\tau_{tot}$  is written as  $\tau_{tot} = \chi\tau_{st} + (1 - \chi)\tau_{local}$ . Furthermore, the relationship between shear stress and  $\dot{\gamma}$  can be described by the Arrhenius equation (Equation (2)). Additionally, in our previous work, a modified yield criterion that considers the pressure sensitivity and strength differential effects is proposed to relate normal stress and shear stress [1]. Based on the above description, the hardness can be written as the function of indentation depth by using the Tabor's relationship between hardness and normal stress [22,41].

#### 5. Conclusions and Remarks

Nanoindentation tests were carried out on aged PMMA to investigate the influences of hygrothermal aging time on its indentation measurements. Based on the test results, the indentation elastic modulus and hardness exhibit a decrease with the increasing aging time, and increase with the strain rate. Additionally, the obvious ISE phenomenon can be observed in aged PMMA, and is found to vary with aging time and indentation strain rate. Finally, a method to quantitatively analyze the ISE of PMMA under different conditions is proposed in present paper, based on shear transformation-mediated plasticity.

**Author Contributions:** Conceptualization, H.L. and T.J.; methodology, T.J.; software, L.L.; validation, H.L., L.L. and T.J.; formal analysis, T.J.; investigation, H.L.; resources, T.J. and H.L.; data curation, L.L.; writing—original draft preparation, H.L.; writing—review and editing, H.L., L.L. and T.J.; supervision, H.L.; project administration, H.L. and T.J.; funding acquisition, T.J. and H.L. All authors have read and agreed to the published version of the manuscript.

**Funding:** This work is supported by the National Natural Science Foundation of China (Grant No. 11802199), Hui Lin would like to acknowledge Shaoxing science and technology project (Grant No. 2018C10005) Tao Jin is grateful to the support from the Open Fund of State Key Laboratory for Strength and Vibration of Mechanical Structures, Xi'an Jiaotong University (SV2019-KF-15). The financial contributions are gratefully acknowledged.

**Conflicts of Interest:** The authors declare no conflict of interest.

#### References

1. Lin, H.; Jin, T.; Lv, L.; Ai, Q. Indentation Size Effect in Pressure-Sensitive Polymer Based on A Criterion for Description of Yield Differential Effects and Shear Transformation-Mediated Plasticity. *Polymers* **2019**, *11*, 412. [[CrossRef](#)] [[PubMed](#)]
2. Jin, T.; Zhou, Z.; Wang, Z.; Wu, G.; Liu, Z.; Shu, X. Quasi-static failure behaviour of PMMA under combined shear-compression loading. *Polym. Test.* **2015**, *42*, 181–184. [[CrossRef](#)]

3. Prokopovich, P.; Köbrick, M.; Brousseau, E.; Perni, S. Potent antimicrobial activity of bone cement encapsulating silver nanoparticles capped with oleic acid. *J. Biomed. Mater. Res. Part B Appl. Biomater.* **2015**, *103*, 273–281. [\[CrossRef\]](#)
4. Vallo, C.I.; Montemartini, P.E.; Fanovich, M.A.; Lopez, J.M.; Cuadrado, T.R. Polymethylmethacrylate-based bone cement modified with hydroxyapatite. *J. Biomed. Mater. Res.* **1999**, *48*, 150–158. [\[CrossRef\]](#)
5. Jin, T.; Zhou, Z.; Wang, Z.; Wu, G.; Shu, X.; Liu, Z. Effects of strain rate on PMMA failure behavior. *Appl. Phys. A* **2016**, *122*. [\[CrossRef\]](#)
6. Shirazi, H.A.; Ayatollahi, M.R.; Naimi-Jamal, M.R. Influence of hydroxyapatite nano-particles on the mechanical and tribological properties of orthopedic cement-based nano-composites measured by nano-indentation and nanoscratch experiments. *J. Mater. Eng. Perform.* **2015**, *24*, 3300–3306. [\[CrossRef\]](#)
7. Su, X.Y.; Zhou, L.; Jing, L.; Wang, H. Experimental investigation and constitutive description of railway wheel/rail steels under medium-strain-rate tensile loading. *J. Mater. Eng. Perform.* **2020**, *29*, 2015–2025. [\[CrossRef\]](#)
8. Jin, T.; Zhou, Z.; Qiu, J.; Wang, Z.; Zhao, D.; Shu, X.; Yan, S. Investigation on the yield behavior of AZ91 magnesium alloy. *J. Alloy. Compd.* **2018**, *738*, 79–88. [\[CrossRef\]](#)
9. Jing, L.; Su, X.Y.; Zhao, L.M. The dynamic compressive behavior and constitutive modeling of D1 railway wheel steel over a wide range of strain rates and temperatures. *Results Phys.* **2017**, *7*, 1452–1461. [\[CrossRef\]](#)
10. Jing, L.; Han, L.L.; Zhao, L.M.; Zhang, Y. The dynamic tensile behavior of railway wheel steel at high strain rates. *Journal of Materials Engineering and Performance. J. Mater. Eng. Perform.* **2016**, *25*, 4959–4966. [\[CrossRef\]](#)
11. Wang, Z.; Qiu, J.; Shu, X.F.; Jin, T. Experimental study on the fracture behavior of AZ91D magnesium alloy under complex loading. *Results Phys.* **2020**, *16*, 102917. [\[CrossRef\]](#)
12. Jing, L.; Su, X.Y.; Yang, F.; Ma, H.W.; Zhao, L.M. Compressive strain rate dependence and constitutive modeling of closed-cell aluminum foams with various relative densities. *J. Mater. Sci.* **2018**, *53*, 14739–14757. [\[CrossRef\]](#)
13. Zhang, J.; Jin, T.; Wang, Z.; Zhao, L. Experimental investigation on yield behavior of PMMA under combined shear-compression loading. *Results Phys.* **2016**, *6*, 265–269. [\[CrossRef\]](#)
14. Qiu, J.; Jin, T.; Su, B.Y.; Shu, X.F.; Li, Z.Q. Experimental investigation on the yield behavior of PMMA. *Polym. Bull.* **2018**, *75*, 5535–5549. [\[CrossRef\]](#)
15. Zhou, Z.; Su, B.; Wang, Z.; Li, Z.; Shu, X.; Zhao, L. Shear-compression failure behavior of PMMA at different loading rates. *Mater. Lett.* **2013**, *109*, 151–153. [\[CrossRef\]](#)
16. Qiu, J.; Jin, T.; Su, B.Y.; Duan, Q.; Shu, X.F.; Liu, E.Q.; Li, X. A Criterion Describing the Dynamic Yield Behavior of PMMA. *Macromol. Res.* **2019**, *27*, 750–755. [\[CrossRef\]](#)
17. Voyiadjis, G.; Malekmoitei, L.; Samadi-Dooki, A. Indentation size effect in amorphous polymers based on shear transformation mediated plasticity. *Polymers* **2018**, *137*, 72–81. [\[CrossRef\]](#)
18. Abdeslam, S. Influence of silver inclusions on the mechanical behavior of Cu-Ag nanocomposite during nanoindentation: Molecular dynamics study. *Results Phys.* **2019**, *15*, 102672. [\[CrossRef\]](#)
19. Pharr, G.; Herbert, E.; Gao, Y. The indentation size effect: A critical examination of experimental observations and mechanistic interpretations. *Annu. Rev. Mater. Res.* **2010**, *40*, 271–292. [\[CrossRef\]](#)
20. Han, C. Influence of the molecular structure on indentation size effect in polymers. *Mater. Sci. Eng.* **2010**, *527*, 619–624. [\[CrossRef\]](#)
21. Hsu, K.C.; Chen, J.Y.; Fang, T.H.; Lin, M.H. Size-dependent strength and interface-dominated deformation mechanisms of Cu/Zr multilayer nanofilms. *Results Phys.* **2018**, *11*, 684–689. [\[CrossRef\]](#)
22. Nix, W.; Gao, H. Indentation size effects in crystalline materials: A law for strain gradient plasticity. *J. Mech. Phys. Solids* **1998**, *46*, 411–425. [\[CrossRef\]](#)
23. Voyiadjis, G.Z.; Song, Y. Strain gradient continuum plasticity theories: Theoretical, numerical and experimental investigations. *Int. J. Plast.* **2019**, *121*, 21–75. [\[CrossRef\]](#)
24. Prasitthipayong, A.; Vachhani, S.J.; Tumey, S.J.; Minor, A.M.; Hosemann, P. Indentation size effect in unirradiated and ion-irradiated 800H steel at high temperatures. *Acta Mater.* **2018**, *144*, 896–904. [\[CrossRef\]](#)
25. Malekmoitei, L.; Samadi-Dooki, A.; Voyiadjis, G.Z. Nanoindentation Study of Yielding and Plasticity of Poly(methylmethacrylate). *Macromolecules* **2015**, *48*, 548–5357. [\[CrossRef\]](#)
26. Zhou, Z.W.; Ma, W.; Zhang, S.J.; Du, H.M.; Mu, Y.H.; Li, G.Y. Multiaxial creep of frozen loess. *Mech. Mater.* **2016**, *95*, 172–191. [\[CrossRef\]](#)

27. Zhou, Z.W.; Ma, W.; Zhang, S.J.; Mu, Y.H.; Li, G.Y. Experimental investigation of the path-dependent strength and deformation behaviours of frozen loess. *Eng. Geol.* **2020**, *265*, 105449. [[CrossRef](#)]
28. Arruda, E.M.; Boyce, M.C.; Jayachandran, R. Effects of strain rate temperature and thermomechanical coupling on the finite strain deformation of glassy polymers. *Mech. Mater.* **1995**, *19*, 193–212. [[CrossRef](#)]
29. Zhou, Z.; Ma, W.; Zhang, S.; Mu, Y.; Li, G. Effect of freeze-thaw cycles in mechanical behaviors of frozen loess. *Cold Reg. Sci. Technol.* **2018**, *146*, 9–18. [[CrossRef](#)]
30. Farrokh, B.; Khan, A. A strain rate dependent yield criterion for isotropic polymers: Low to high rates of loading. *Eur. J. Mech. Solids* **2010**, *29*, 274–282. [[CrossRef](#)]
31. Jin, T.; Zhou, Z.; Liu, Z.; Xiao, G.; Yuan, G.; Shu, X. Sensitivity of PMMA nanoindentation measurements to strain rate. *J. Appl. Polym. Sci.* **2015**, 41896. [[CrossRef](#)]
32. Oyen, M. Sensitivity of polymer nanoindentation creep measurements to experimental variables. *Acta Mater.* **2007**, *55*, 3633–3639. [[CrossRef](#)]
33. Xiao, G.S. Mechanical Properties of Cured Isotropic Conductive Adhesive Investigated by Micro-Indentation. Ph.D. Thesis, Taiyuan University of Technology, Taiyuan, China, 13 June 2015. (In Chinese).
34. Ma, Y.; Ye, J.; Peng, G.; Wen, D.; Zhang, T. Nanoindentation study of size effect on shear transformation zone size in a Ni-Nb metallic glass. *Mater. Sci. Eng. A* **2015**, *627*, 153–160. [[CrossRef](#)]
35. Spaepen, F. A microscopic mechanism for steady state inhomogeneous flow in metallic glasses. *Acta Mater.* **1977**, *25*, 407–415. [[CrossRef](#)]
36. Argon, A. Plastic deformation in metallic glasses. *Acta Mater.* **1979**, *27*, 47–58. [[CrossRef](#)]
37. Poisl, W.; Oliver, W.; Fabes, B. The relationship between indentation and uniaxial creep in amorphous selenium. *J. Mater. Res.* **1995**, *10*, 2024–2032. [[CrossRef](#)]
38. Schuh, C.; Nieh, T. A nanoindentation study of serrated flow in bulk metallic glasses. *Acta Mater.* **2003**, *51*, 87–99. [[CrossRef](#)]
39. Schuh, C.; Lund, A.; Nieh, T. New regime of homogeneous flow in the deformation map of metallic glasses: Elevated temperature nanoindentation experiments and mechanistic modeling. *Acta Mater.* **2004**, *52*, 5879–5891. [[CrossRef](#)]
40. Cheng, Y.T.; Cheng, C.M. Scaling, dimensional analysis and indentation measurements. *Mater. Sci. Eng. R.* **2004**, *44*, 91–149. [[CrossRef](#)]
41. Lam, D.; Chong, A. Indentation model and strain gradient plasticity law for glassy polymers. *J. Mater. Res.* **1999**, *14*, 3784–3788. [[CrossRef](#)]



© 2020 by the authors. Licensee MDPI, Basel, Switzerland. This article is an open access article distributed under the terms and conditions of the Creative Commons Attribution (CC BY) license (<http://creativecommons.org/licenses/by/4.0/>).